How Well Do Molecular Dynamics Force Fields Model Peptides? A Systematic Benchmark Across Diverse Folding Behaviors

Bhumika Singh,[†,¶] Yisel Martínez-Noa,[†,¶] and Alberto Perez[*,†,‡]

†*Department of Chemistry, University of Florida, Gainesville, FL, USA*

‡*Quantum Theory Project, University of Florida, Gainesville, FL, USA*

¶*These authors contributed equally to this work*

E-mail: perez@chem.ufl.edu

Abstract

Linear peptides play essential roles in biology and drug discovery, frequently mediating protein–protein interactions through short, flexible motifs. However, their structural plasticity—ranging from disordered to context-dependent folding—makes them challenging targets for molecular simulations. In this work, we benchmark the performance of twelve popular and emerging fixed-charge force fields across a curated set of twelve peptides spanning structured miniproteins, context-sensitive epitopes, and disordered sequences. Each peptide was simulated from both folded (200 ns) and extended (10 μs) states to assess stability, folding behavior, and force field biases. Our analysis reveals consistent trends: some force fields exhibit strong structural bias, others allow reversible fluctuations, and no single model performs optimally across all systems. The study highlights limitations in current force fields' ability to balance disorder and secondary structure, particularly when modeling conformational selection. These results

offer practical guidance for peptide modeling and establish a benchmark framework for future force field development and validation in peptide-relevant regimes.

Introduction

Peptide epitopes—short regions within proteins that mediate molecular recognition—play central roles in biology and drug discovery. Many cellular interactions are driven by such short linear motifs[1,2], which bind to specific partner proteins and often undergo disorder-to-order transitions in the process[3]. This structural plasticity is both biologically important and a significant modeling challenge.

Peptides are particularly attractive drug candidates because they can engage extended and shallow protein surfaces that are typically inaccessible to small molecules[4]. Advances such as peptide cyclization have improved their proteolytic stability and membrane permeability, further boosting their therapeutic potential[5]. Accurate modeling of peptide structure and binding is thus crucial for structure-based design of peptide therapeutics, peptidomimetics, and small molecules that mimic peptide–protein interactions.

Yet, modeling peptides remains difficult. Many peptides are intrinsically disordered in isolation and only fold upon binding to a target[6,7]. Others form defined secondary structures under specific solution conditions, but not others[8,9]. A singular protein receptor might recognize different peptide sequences via distinct binding modes (e.g., peptide binds as a helix or hairpin)[10], while a given peptide sequence may bind different protein receptors by adopting different structures[11,12]. This environmental sensitivity places peptides near the edge of structural stability, where small changes in sequence, solvent, or receptor can trigger large conformational shifts. Unlike globular proteins, which are stabilized by dense networks of non-bonded interactions, peptides often lack such extensive stabilizing contacts[13,14]. As a result, even small inaccuracies in the force field can lead to significant errors in conformational preferences[15–17].

From a computational standpoint, peptides are small enough that conformational sampling is not generally a limiting factor. However, their responsiveness to small perturbations makes them especially susceptible to force field biases[18–20]. For instance, modest secondary structure preferences encoded in a force field may not strongly affect the native fold of a protein but can dominate the ensemble of a flexible peptide[21]. Despite recent improvements, traditional force fields were largely developed and parameterized to describe well-folded proteins, often leading to over-compact ensembles for disordered systems.

Increasing computer time and access to better benchmark experimental data have shown several force field deficiencies, such as inaccurate helical propensities or incorrect compaction in disordered proteins[22,23]. This has led to an explosion in the number of groups participating in force field development as well as the number of available force fields. Yet, many of these developments have focused on large protein systems, and it remains unclear which force fields best describe peptides across different structural regimes[24,25].

In this work, we systematically assess the performance of 11 modern force fields across a benchmark set of 12 peptides. These include peptides that are structured in solution, intrinsically disordered peptides, and peptides that remain disordered in water but fold in alternative solvent environments. We evaluate both structure stability (via simulations initiated from folded states) and folding behavior (via simulations initiated from extended conformations). While no force field performs optimally in all cases, our results reveal meaningful trends and biases, offering practical guidance for researchers modeling peptide-mediated interactions.

Computational Methods

Systems of study

A total of twelve peptides (see Table 1) were selected as model systems to evaluate and compare force fields.

Table 1: Benchmark systems used in this study.

Name	PDB ID	Method	Sequence
Miniproteins			
tc5b	1L2Y[26]	NMR	NLYIQWLKDGGPSSGRPPPS
tryptophan zipper 2	1LE1[27]	NMR	SWTWENGKWTWK
human beta-defensin-1	1IJU[28]	X-ray	DHYNCVSSGGQCLYSACPIFTKIQGT CYRGKAKCCK
Partially Structured Peptides			
protein G C-termini	1GB1[29]	NMR	GEWTYDDATKTFTVTE
ribonuclease A C-peptide analog	5RSA[30]	X-ray	AETAAAKFLRAHA
EK peptide	–	CD[31]	YAEAAKAAEAAKAF
Structured Upon Binding			
matα2	1MNM[32]	X-ray	VFNVVTQDMINKST (Residue 115–128)
nrf2 peptide	2FLU[33]	X-ray	AFFAQLQLDEETGEFL
dynorphin A	2N2F[34]	NMR	YGGFLRRIRPKLK
Disordered in Water, Ordered in Solvent Mixtures			
glucagon-like peptide-1-(7–36)-amide	1D0R[35]	NMR	HAEGTFTSDVSSYLEGQAAKEFIAWL VKGR
proadrenomedullin N-20 terminal	2FLY[36]	NMR	ARLDVASEFRKKWNKWALSR
phylloseptin-1	2JQ0[37]	NMR	FLSLIPHAINAVSAIAKHNX

Force field choices

We took some traditional force fields ff19SB,[38] ff99SB,[39] and charmm36m[40] commonly used in the field, as well as some IDP optimized force fields ff99IDPs,[41] ff14IDPs,[42]ff14IDPSFF,[43] C36IDPSFF,[44] OPLDIDPSFF,[45] and some physics-enhanced modern force fields a99SBdisp,[15] Des-Amber.[46] For each force field, we used the water model recommended for it (see table 2). While this is not an exhaustive list of force fields, it is representative of different trends in the field and readily available for running simulations.

Table 2: Summary of force fields and water models employed in this benchmark study.

Forcefield	**Water Model**
ff19SB	OPC[47]
ff99SB	OPC[47]
ff99IDPs	TIP3P[48]
ff14IDPs	TIP3P[48]
ff14IDPSFF	TIP3P[48]
OPLSIDPSFF	TIP4P[48]
a99SBdisp	a99SBdisp-water[15]
DES-Amber	TIP4P-D[49]
DES-Amber-SF1.0	TIP4P-D[49]
Charmm36m	TIP3P[48]
C36IDPSFF	TIP3P[48]

Simulation protocols

Molecular dynamics simulations were performed using twelve force fields, including variants incorporating CMAP corrections. The force fields examined in this study, along with their recommended water models, are summarized in Table 2. Molecular dynamics simulations were conducted using GROMACS[50] and Amber,[51,52] according to the availability of the corresponding force field. We use hydrogen mass repartitioning with a 4 fs timestep, and we saved frames every 20ps. Simulations initiated from the unfolded state ran for 10 μs and those starting from the folded state ran for 200 ns.

AMBER protocols

For the AMBER simulations, we solvated the systems employing tleap with the initial parameters of the force fields ff14SB[53], ff99SB, and f19SB initially, and the peptides were solvated in 8 Å water buffer in a truncated octahedron. We used cloride or sodium neutralizing ions and brought up their concentration to $0.1M$, randomizing their positions. For the force fields ff14IDPs and ff14IDPsFF, we first initialized the systems using ff14SB pa-

rameters and subsequently applied the corresponding CMAP corrections. Similarly, systems using ff99IDPs were initialized with ff99SB and then updated with the CMAP corrections specific to ff99IDPs. For charmm36m we prepared our input through the CHARMMGUI platform[54–56], using the solution builder input generator, likewise we add sodium and chlorine ions in an 8 Å water octahedron box. All minimization steps were performed using the sander module from AMBER20[51]. A series of restrained energy minimizations were conducted to gradually relax the system while maintaining the structural integrity of the solute. The protocol involved six sequential minimization steps with harmonic positional restraints applied to all non-hydrogen atoms of the solute, progressively decreasing the restraint weight from 50 $\mathrm{kcal\,mol^{-1}\,\AA^{-2}}$ to 5 $\mathrm{kcal\,mol^{-1}\,\AA^{-2}}$ in increments of 10 $\mathrm{kcal\,mol^{-1}\,\AA^{-2}}$. The final minimization step was performed without restraints. Each minimization was carried out using 4000 total steps, with the first 2000 steps utilizing steepest descent, followed by conjugate gradient minimization for the remaining steps. Restraints were applied to all atoms except hydrogen and water molecules. The system was first thermalized over 5 ns, gradually increasing the temperature from 0 K to 298.15 K using Langevin dynamics[57–59] with a collision frequency of 1 ps^{-1} to control temperature fluctuations. Following this, a 10 ns equilibration step was carried out with positional restraints on the solute and periodic boundary conditions were enforced. Additionally, a second equilibration was performed for an additional 10 ns at constant pressure of 1 atm using the Berendsen barostat[60]. Temperature control continued through Langevin dynamics, with an increased collision frequency of 2 ps^{-1}. Finally, the MD simulations of 10 μs for the systems initiated from the unfolded state and 200 ns for the systems initiated from the experimentally folded state, were run with a 4 fs time step.

GROMACS protocols

Simulations using the OPLSIDPSFF,[45] a99SBdisp,[15] DES-Amber,[46] DES-Amber-SF1.0,[46] and C36IDPSFF[44] force fields were performed with GROMACS version 2019.2[50]. To ensure

consistency with the AMBER-based simulations, similar protocols and conditions were applied across all systems. For simulations initiated from the unfolded state extended linear conformations were generated using the *xleap* module in AMBER. In contrast, folded-state simulations were based on experimentally determined structures retrieved from the RCSB Protein Data Bank (PDB).[61] Each peptide's topologies and coordinates were prepared separately for each force field. Each system was solvated in a truncated octahedral box using the water model recommended for the respective force field (see Table 2), maintaining at least 8 Å of padding between the solute and the box boundaries. Sodium (Na^+) and chloride (Cl^-) ions were added to neutralize the system and to achieve a final salt concentration of 0.1M.

Energy minimization was performed in two stages: an initial steepest descent minimization of up to 50,000 steps, followed by 2,000 steps of conjugate gradient minimization[62]. The systems were then gradually heated to 300 K over 10 ns in the canonical (NVT) ensemble, followed by a 20 ns equilibration in the isothermal-isobaric (NPT) ensemble. Covalent bonds involving hydrogen atoms were constrained using the LINCS algorithm[63]. Lennard-Jones and short-range electrostatic interactions were truncated at 10 Å. Long-range electrostatics were treated using the Particle Mesh Ewald (PME) method[64]. Temperature was controlled using the velocity-rescale thermostat set at 300 K, and pressure was maintained at 1 atm using the Parrinello-Rahman barostat[65,66].

Finally, simulations were conducted with a 2 fs integration time step during the heating and equilibration phases. After applying hydrogen mass repartitioning[67], the time step was increased to 4 fs during production. For each force field, production simulations of 10 μs were performed for the unfolded systems, while 200 ns simulations were conducted for systems starting from folded PDB structures.

Following the simulations, we utilized the cpptraj[68,69] and MDAnalysis[70,71] tools for the analysis step, and VMD[72] for the visualization and trajectory analysis.

Analysis

Ramachandran Plots

To evaluate the stereochemical quality and conformational preferences of amino acid residues within the peptide sequences, Ramachandran[73] plots were generated. These plots provide a visual representation of the backbone dihedral angles (ϕ and ψ), offering insights into the propensity of residues to adopt specific secondary structural elements such as α-helices, β-sheets, or random coils. The analysis was performed using the `MDAnalysis` toolkit, employing the `Ramachandran` class to compute ϕ and ψ angles across all residues over time. Stripped and aligned trajectories, along with the corresponding topology files, were used as input to ensure accurate dihedral angle calculations.

Clustering

To identify representative conformations and their populations sampled during the simulations, structural clustering was performed on each trajectory for every force field and system. Hierarchical agglomerative clustering with average linkage was applied using an RMSD-based metric with an ϵ cutoff of 3.0 Å, as implemented in `cpptraj`, part of the `AmberTools` suite. For the 10 μs simulations, every 50th frame was extracted; for the 200 ns simulations, all frames were used. Clustering was based on the backbone heavy atoms (C, N, O, Cα, and Cβ) of all peptide residues. Cluster centroids were selected as representative structures. Notably, inclusion of all residues led to similar conformations being distributed across multiple clusters in some cases, likely due to increased flexibility in loop regions.

Secondary Structure preferences

Secondary structure content of the simulated peptides was analyzed using the `secstruct` command in `cpptraj`. Prior to analysis, trajectories were preprocessed with the autoimage command to correct for periodic boundary conditions and maintain peptide chain continuity.

Secondary structure assignment was carried out using the DSSP algorithm[74] as implemented in `cpptraj`, which classifies structural elements—including α-helices, β-strands, turns, and coils—based on backbone hydrogen bonding patterns and geometric features.

Conformational Diversity and Structural Deviation Analysis

To quantify the conformational diversity sampled by each force field, Shannon entropy[75] was calculated based on the fractional populations of clusters obtained from the hierarchical clustering analysis (as described in the *Clustering* section). This metric captures the degree of structural heterogeneity within a simulation, where higher entropy values indicate greater conformational diversity. Entropy, S, was calculated using the following equation:

$$S = -\sum_i P_i \log P_i$$

where P_i is the population fraction of the i-th cluster. Calculations were performed with the `pandas`[76] and `NumPy`[77] Python libraries.

To assess structural deviations from the native state, root-mean-square deviation (RMSD) was computed for the most populated cluster for each force field in each system. The reference structure corresponded to the experimentally determined folded state of the peptide. RMSD was calculated using the backbone heavy atoms (C, N, O, Cα, and Cβ) of all residues, employing `cpptraj` from the AmberTools suite.

Results

Systems of study

The structural characterization of peptides presents a particularly stringent test for molecular force fields. While most peptide sequences are intrinsically disordered in solution, certain peptides have been experimentally observed to adopt defined secondary structures under

specific conditions—such as binding to a partner protein, folding in a membrane-mimetic solvent, or being excised from a larger folded domain. These context-dependent peptides occupy an intermediate regime between fully folded miniproteins and disordered chains, making them ideal benchmarks for assessing force field accuracy and bias. We selected twelve experimentally characterized peptides that span four categories: (1) miniproteins with well-defined structures in solution, (2) partially structured peptides, (3) peptides that fold upon binding to a protein target, and (4) disordered peptides that adopt defined structure only in membrane-mimetic or mixed solvents. This set (see Fig. 1) enables us to evaluate force field performance across a biologically meaningful spectrum of structural propensities.

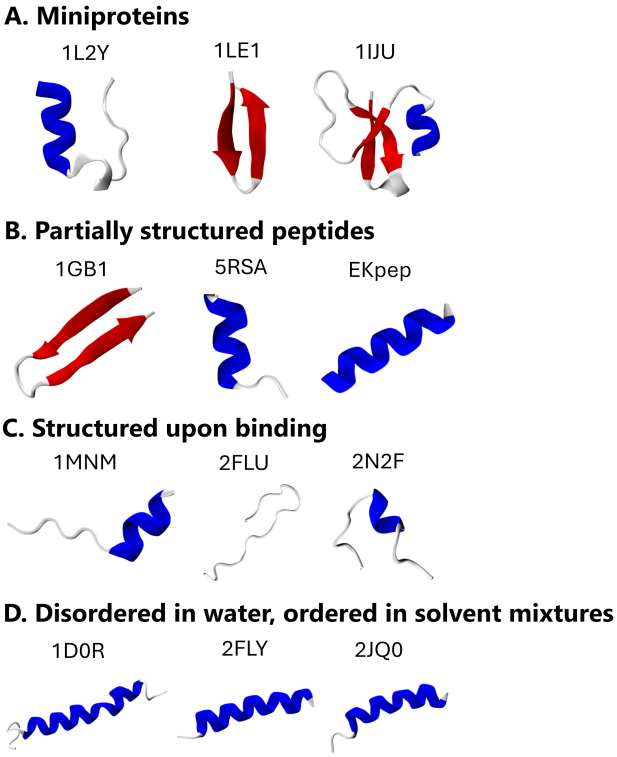

Figure 1: **Experimentally folded structures of benchmark peptide systems used in this study, shown with their corresponding PDB IDs.**

Miniproteins: These peptides adopt well-defined, compact tertiary folds under aqueous conditions and are considered stable, folded entities in solution. Trp-cage (1L2Y) is often classified as a miniprotein, as it exhibits over 95% folded population at physiological

pH, forming a compact helical bundle stabilized by a hydrophobic core nucleated around a tryptophan residue.[26] This 20 residue sequence was optimized starting from a 39 residue protein. Trp-zip (1LE1) is a 13-residue *de novo* designed sequence that folds as a β-hairpin. Four tryptophan residues create a hydrophobic side in the hairpin, while polar and charged residues are present in the other side. Trp-zip is highly stable with high hairpin populations (>95%) in water, as confirmed by NMR.[27] Finally, β-defensin-1 (1IJU) is a natural antimicrobial peptide that forms stable monomers and dimers in crystallographic studies. NMR of a homologous defensin confirms that monomeric structure is preserved in dilute solution.[28,78] This 36 residue sequence is the longest in our dataset.

Partially structured peptides: These peptides exhibit some degree of structure in solution, often sampling a mixture of folded and unfolded conformations. Two of them are fragments derived from larger proteins, whereas the third one is a designed peptide. The C-termini from Protein G (β-hairpin, 1GB1) is a 16-residue segment from the immunoglobulin binding domain of streptococcal protein G. This hairpin is expected to be formed early in protein G folding[79] and experimental studies suggests that this peptide should adopt ∼20% hairpin population in solution.[27]C-peptide (helical, 5RSA) is a 13-residue analog from the RNase A N-terminal with moderate α-helical content in water. The original C-termini had a small helical population in solution and analogs produced with sequence optimization increased the helical stability with populations ranging from 40–60% depending on temperature and variant.[80,81] The EK peptide is a designed helical peptide with favorable electrostatics (E,K at $i, i+4$ positions). Circular dichroism (CD) studies estimate 40% helical population in solution.[82] The AlphaFold[83] prediction is used as a reference.

Structured upon binding: These peptides are expected to be disordered or dynamic in isolation but adopt specific folded conformations upon binding to a protein receptor. The MATα2 epitope (1MNM) is a context-dependent peptide from MATα2 (residues 115-128) that has been observed binding as both a helix or a hairpin in the same crystal structure.[32]

This unique chameleon-like behavior is a practical test case for our force fields. The NRF2 peptide (2FLU) forms a small β-hairpin motif when bound to the Kelch domain of KEAP1.[33] Its unbound conformation is not structurally characterized, making it a useful test for detecting folding bias. The dynorphin A peptide (2N2F) binds the human κ-opioid receptor (KOR) as a structured peptide (residues 1-13 from dynorphin A) with a central helical motif, flanked by disordered termini.[34]

Disordered in water, ordered in solvent mixtures: These systems adopt helical structure in mixed solvent environments such as Trifluoroethanol (TFE)/water or membrane mimetics but remain disordered in pure water. They serve as sensitive probes for helical bias. The glucagon-like peptide-1 (GLP-1, 1D0R) is a peptide hormone that is unstructured in water but adopts a helix in 35% TFE. NMR experiments at different TFE concentrations shows that the C-terminal region has a higher helix propensity.[35] The PAMP peptide (2FLY) also exhibits α-helicity in both membrane mimetic and TFE environments according to NMR studies.[36] Finally, Phylloseptin-1 (2JQ0) is an antimicrobial peptide whose helical population increases with TFE concentration—from 53% at 30% to 70% at 60%.[37]

To evaluate force field performance for these systems, we conducted two sets of simulations for each system: 1) Short simulations (200 ns) initiated from the experimentally determined or AlphaFold-predicted (EK peptide) structure, to assess structural stability and strong biases. 2) Long simulations (10 μs) initiated from extended conformations, to assess folding tendencies, sampling breadth, and subtle biases.

Each system's simulation outputs— Ramachandran analysis, secondary structure propensities, cluster entropy, RMSD trajectories, representative conformers—are summarized in the main text and detailed in Supplementary Figures S1–S60. These results guide our analysis of force field accuracy and conformational bias.

Modeling peptide stability

Short, 200 ns simulations starting from a folded conformation provide a practical means to detect strong force field biases. While unfolding proteins and nucleic acids in explicit solvent simulations in denaturing solvent mixtures requires long timescales,[84,85] peptides—due to their smaller size and limited stabilizing contacts—can unfold spontaneously within this timescale, especially when the native structure is marginally stable or environment-dependent.[84,85] Thus, we use this protocol to detect whether force fields maintain starting structural features or quickly deviate toward alternative states.

Miniproteins

For the three miniproteins (1L2Y, 1LE1, 1IJU), all of which are expected to remain stably folded in solution, most force fields preserve native structure throughout the simulation. Trp-cage (1L2Y) retains its compact helical bundle in most force fields, though ff99IDPs, OPLSIDPs, and ff14IDPSFF show partial helix loss (SI Fig.1-4). Trpzip (1LE1), a highly stable β-hairpin, is preserved in all force fields except ff99IDPs, which fails to maintain the strand pairing (SI fig 6-9). For β-defensin (1IJU), which is the longest sequence in our set and not a designed miniprotein, most force fields retain the native-like β-sheet, though IDP-biased force fields (ff99IDPs, ff14IDPs, ff14IDPSFF, C36IDPSFF) along with Charmm36m show partial unfolding (SI fig. 11-14). ff99IDPs maintains some regions of strand pairings but loses the overall fold. Some force fields (ff14IDPSFF, Charmm36m, and C36IDPSFF) lose the N-terminal helix at least partially, as observed in β-defensin2.

Partially structured peptides

These peptides (1GB1, 5RSA, EK) are expected to adopt partially folded conformations. In this short timescale we expect that either the structure could be either stabilized totally or partially. We do not necessarily expect to see unfolding and refolding in this short timescale. In 1GB1, a fragment from protein G, all force fields maintain the native β-hairpin in this short

timescale, consistent with experimental data pointing to the presence of folded structures in the ensemble. Ff99IDPs is the only exception, where the tail of the hairpin is lost for most of the trajectory, with short lived helical turns forming in those regions (seef SI Fig 16-19). For C-peptide (5RSA), approximately half of the force fields lose helicity early in the simulation (SI Fig. 21-24). a99SBdisp and ff99IDPs show unfolding and partial refolding behavior, while Charmm36m transitions to a β-hairpin-like state in the final 40 ns. For EK, a designed helix, several force fields (including OPLSIDPSFF and Charmm36m) lose the structure entirely and do not recover it, while ff19SB and ff99IDPs show unfolding followed by partial refolding (SI Fig. 26-29). Interestingly, OPLSIDPSFF samples β-hairpin-like states near the end of the trajectory, indicating a possible strand-biased artifact.

Structured upon binding

These peptides (1MNM, 2FLU, 2N2F) fold only upon receptor binding and are expected to show low stability as isolated monomers. For 1MNM, which was started in the helical form but can also adopt a hairpin when bound, most force fields unfold the helix, with only ff19SB, a99SBdisp, and des-amber-SF1.0 retaining structure (SI Fig. 31-34). Some (ff99IDPs, ff14IDPs) transiently refold the helix. NRF2 (2FLU) is maintained as a short c-termini hairpin in C36IDPSFF, charmm36m, and ff14IDPSFF. Ff19SB and ff99SB stabilize it for the first part of the trajectory – with ff99SB sampling helical states the second half of the trajectory (see SI Fig. 36-39). FF99IDPs and ff14IDPSFF have helical tendencies, with the remaining force fields adopting almost no secondary structure for the whole trajectory. For 2N2F, the central helix is rapidly lost in most simulations, with only a few force fields showing transient recovery of the folded motif (ff19SB, a99SBdisp, des-amber-SF1.0, and ff14IDPs) (SI Fig. 41-44). Additionally, ff14IDPs sampled short hairpin states.

Solvent-sensitive helices

The last group comprises peptides (1D0R, 2FLY, 2JQ0) (SI Fig. 46-60) that form helices in membrane-mimetic or TFE-containing solvents but are disordered in water. Several force fields lose helical structure rapidly, and some maintain it during most or all of the simulation length – at least partially. However, ff99IDPs occasionally samples β-hairpin conformations in 2FLY and 2JQ0, suggesting a mild β-bias. These results indicate that force fields with strong secondary structure biases may alter the misfolding landscape even when the native state is unstructured.

Summary. Taken together, these 200 ns simulations reveal consistent trends across peptide classes (Fig. 2 and SI Table 1). Force fields such as ff19SB and a99SBdisp strike a balance between stability and flexibility, maintaining expected structure in miniproteins and partially structured peptides while allowing partial unfolding in binding-induced and solvent-sensitive systems. In contrast, ff99IDPs frequently destabilizes folded helices and occasionally introduces β-structures in non-β contexts. OPLSIDPSFF and Charmm36m show occasional strand-bias, highlighting how tuning for disordered ensembles can influence the behavior of context-sensitive peptides.

Modeling peptide folding

While short simulations reveal whether force fields preserve native structures, they cannot assess whether force fields can discover such conformations from unfolded states. We therefore turn to long-timescale simulations initiated from extended conformations to examine folding behavior, landscape preferences, and potential biases in structural sampling (10 µs). This approach helps detect dominant basins in the energy landscape and potential biases—e.g., force fields that prefer β-hairpins across many sequences or that stabilize incorrect folds once visited.

Some peptides that appeared disordered in the 200 ns simulations now display unexpected

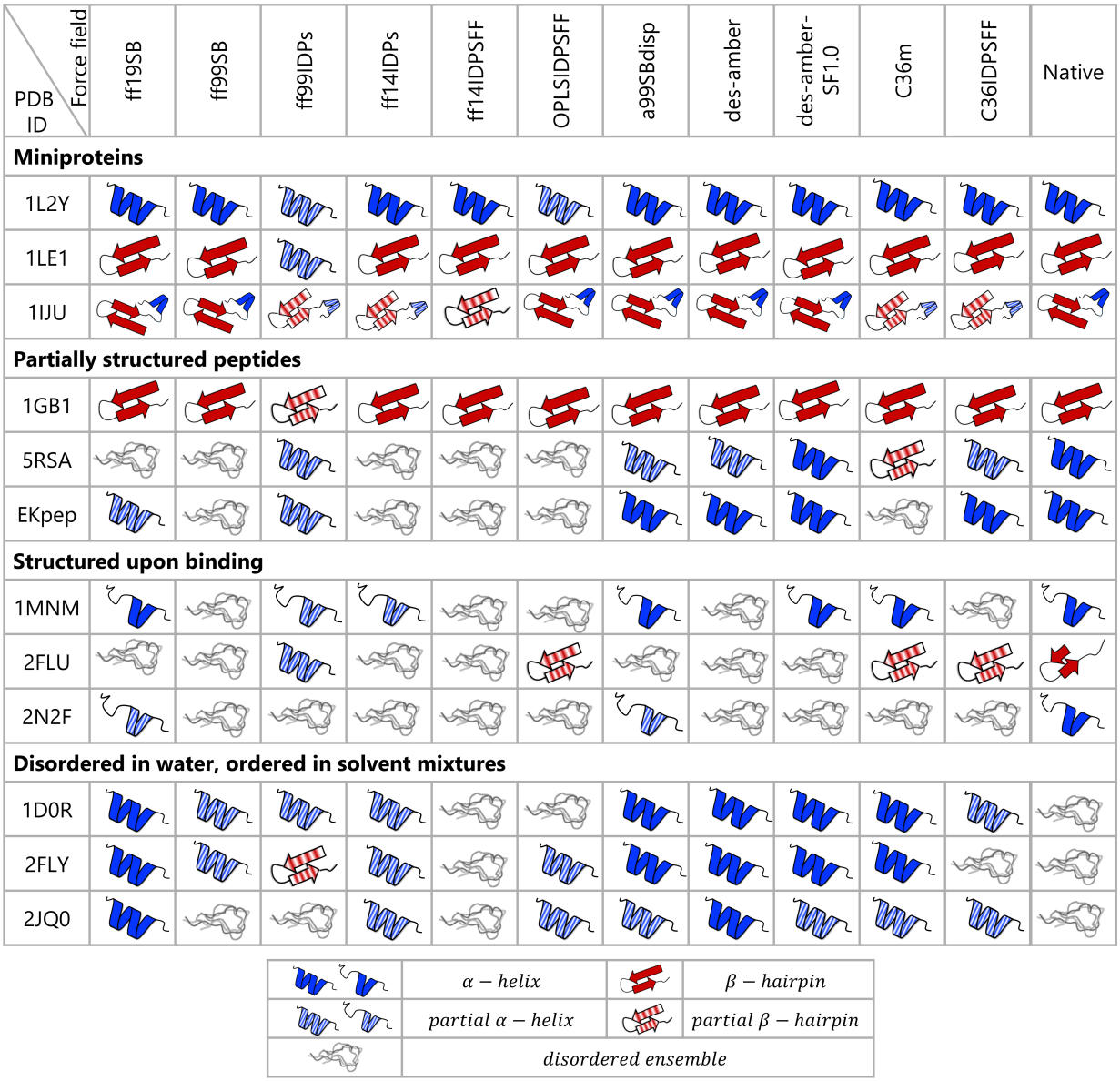

Figure 2: **Summary of the overall trends observed for each force field across different systems during 200 ns simulations initiated from experimentally folded structures.** Solid-colored helices or hairpins represent stable native secondary structures, while striped representations indicate partial retention or stabilization of non-native secondary structures. Wavy lines denote disordered ensemble sampling.

structure preferences, with certain force fields systematically promoting strand pairing or helix formation. Conversely, some force fields fail to reach native-like states for peptides known to be structured. Notably, OPLSIDPSFF frequently stabilizes β-hairpins early and maintains them, regardless of the peptide's native fold. Force fields such as ff19SB and ff99IDPs often revisit native-like helices intermittently, suggesting balanced sampling.

Miniproteins

Trp-cage (1L2Y), with two helical regions, is folded only by ff19SB and a99SBdisp, with the former stabilizing the structure longer. OPLSIDPSFF and several others prefer β-hairpin-like folds, indicating non-native bias (SI Fig. 1-5). For Trpzip (1LE1), a highly stable β-hairpin, six force fields fold the correct structure within 2.5μs (SI Fig. 6-10). ff14IDPS initially folds a β-hairpin but then samples and stabilizes a helical motif. The longest peptide in this set, β-defensin-1 (1IJU), remains unfolded across all force fields (SI Fig. 11-15). OPLSIDPSFF again stand out by stabilizing a non-native three-stranded β-sheet, while others sample isolated elements of native structure without convergence into the native fold.

Partially structured peptides

EK and C-peptide (5RSA) both exhibit moderate helical content experimentally. ff19SB and ff99IDPs are the only force fields that consistently sample and stabilize helical conformations for both peptides (SI Fig 21-30). OPLSIDPSFF favors hairpin states instead. Interestingly, these same force fields (ff19SB and ff99IDPs) partially lost helicity in 200 ns stability simulations—suggesting that their ability to unfold and refold reflects a relatively unbiased, physically realistic ensemble rather than a strong bias towards helical states.

For the Protein G C-terminal hairpin (1GB1), only OPLSIDPSFF successfully folds the hairpin within the first 100 ns and maintains it throughout the simulation. This is reflected in its clustering analysis, which reveals a single dominant state comprising over 80% of the trajectory. In contrast, ff14IDPs and ff99IDPs favor helical conformations for much of the

trajectory, but without consistent convergence—top cluster populations are only ∼10% and ∼20%, respectively. The remaining force fields sample structurally diverse ensembles with little secondary structure (SI Figs. 16–20). Notably, des-amber, C36mIDPsFF, and ff14IDPs populate hairpin-like states frequently enough for them to define the most populated cluster, although these clusters still represent less than 15% of the total ensemble.

Structured upon binding

These peptides are unstructured in isolation but adopt defined folds when bound to protein partners. Their behavior in extended simulations is highly force field-dependent.

The MATα2 chameleon peptide (1MNM) exhibits divergent behavior: ff99SB, and ff99IDPs sample both helix and hairpin conformations sparingly, while other force fields show preference for either helix (ff19SB, ff14IDPs, a99SBdisp) or β-structure (OPLSIDPSFF). Other force fields adopt secondary structure sparingly (SI Fig. 31-35). For NRF2 (2FLU), OPLSIDPSFF stabilizes a non-native β-hairpin, four force fields (ff19SB, ff99IDPs, ff14IDPs, and ff14IDPSFF) exhibit helical tendencies, and the remaining form secondary structure sparingly, with C36IDPsFF stabilizing a native-like hairpin with low population (SI Fig. 36-40). In 2N2F, ff19SB samples native helical motifs at low populations, while most others show low degrees of secondary structure (SI Fig. 41-45). Despite this, clustering indicates convergence: top clusters are highly populated and structurally similar to each other and to stability simulations, suggesting a shared ensemble.

Solvent-sensitive helices

Peptides such as GLP-1 (1D0R), PAMP (2FLY), and phylloseptin-1 (2JQ0) adopt helices only in TFE or membrane mimetic conditions and are expected to remain disordered in pure water. Force fields that introduce structured states in this regime indicate potential over-structuring.

Across all three peptides, ff14IDPSFF and OPLSIDPSFF frequently stabilize β-hairpin-

like motifs. To a lesser extent, C36IDPSFF and ff99IDPs show similar behavior. In contrast, ff19SB, des-amber, and des-amber-SF1.0 promote helicity in 1D0R and 2FLY, particularly in the C-terminal region—consistent with NMR (SI Fig 46-55). 2JQ0 shows lower helical content overall (SI Fig. 56-60).

Summary. Folding simulations highlight distinct tendencies among force fields (Fig. 3 and SI Table 2). OPLSIDPSFF displays a strong and consistent β-bias across systems, often producing dominant clusters regardless of peptide identity. ff19SB and ff99IDPs show context-sensitive behavior, folding miniproteins and moderately structured peptides while avoiding strong misfolding. IDP-optimized force fields vary widely in behavior: some (ff14IDPSFF) promote β-structure, while others (ff99IDPs) show flexibility and helix recovery. These simulations emphasize the need to assess force field performance across multiple structural regimes and not assume generality based on protein-focused benchmarks.

Across nearly all peptides, OPLSIDPSFF shows a consistent β-hairpin preference, often early in the trajectory (e.g., 1GB1, EK, 1D0R), leading to dominant cluster populations (e.g., 1GB1: $> 80\%$). In contrast, ff19SB and ff99IDPs intermittently recover native-like helices in marginal systems (e.g., EK, 5RSA), suggesting balanced behavior.

Entropy as a proxy for conformational sampling across force fields

Entropy derived from population-weighted cluster occupancies using Shannon's entropy offers a compact way to compare the breadth and distribution of conformational space explored by different force fields. Because both system size and trajectory length modulate the absolute value, we treat the 200 ns native-start and 10 µs extended-start ensembles separately (Fig. 4 and SI Figs. 61-62). Our objective is not exhaustive sampling, but rather to identify systematic force field tendencies—whether they artificially constrain (low entropy) or overly-disperse (high entropy) the ensemble.

We interpret the entropy-RMSD landscape (see Fig. 4) using three qualitative regimes:

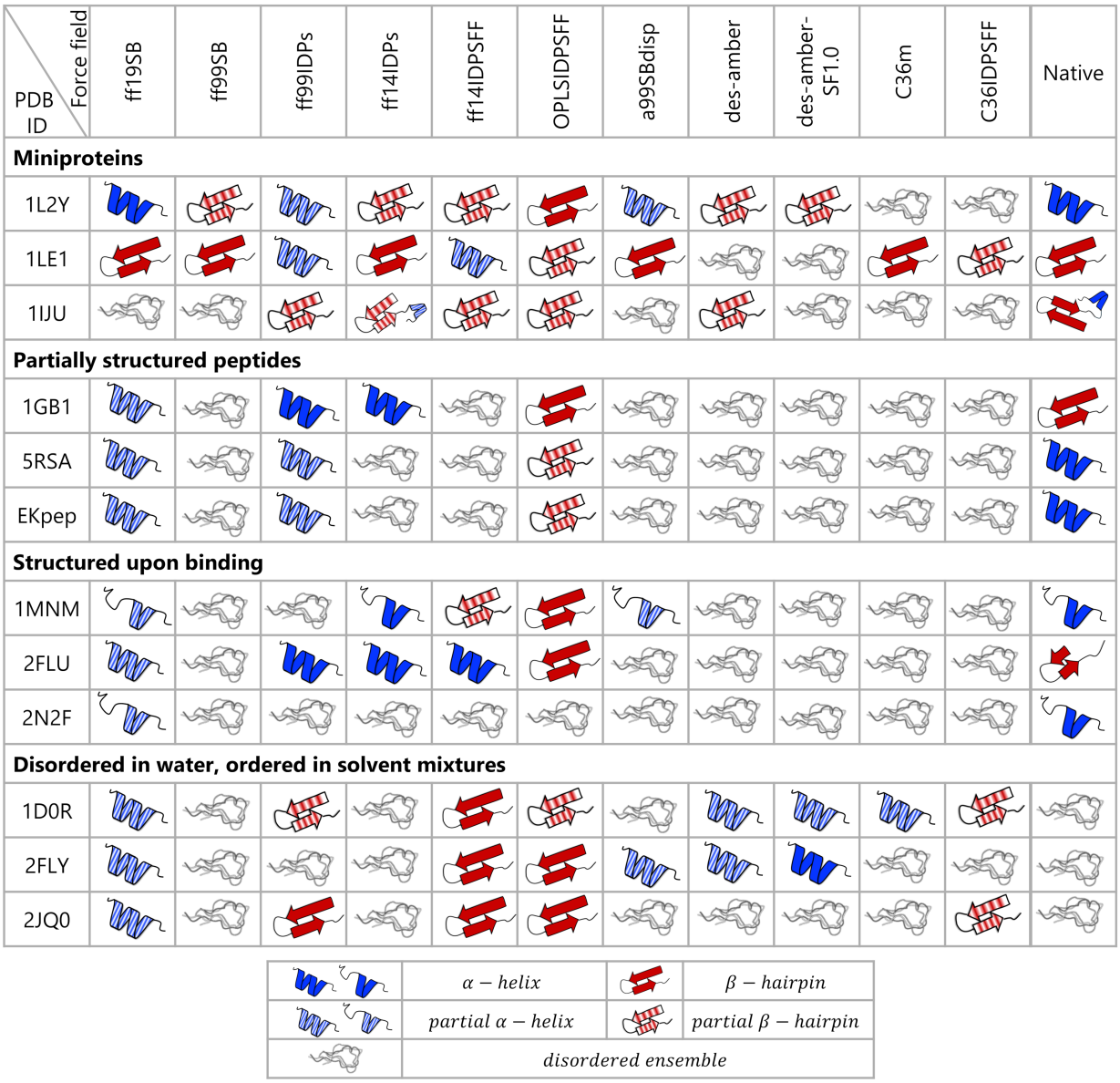

Figure 3: **Summary of overall trends observed for each force field across different systems during 10 μs simulations initiated from linear peptide sequences.** Solid-colored helices or hairpins represent the formation of native secondary structures, while striped helices or hairpins indicate partial formation of native structures or stabilization of non-native secondary structures. Wavy lines denote disordered ensemble sampling.

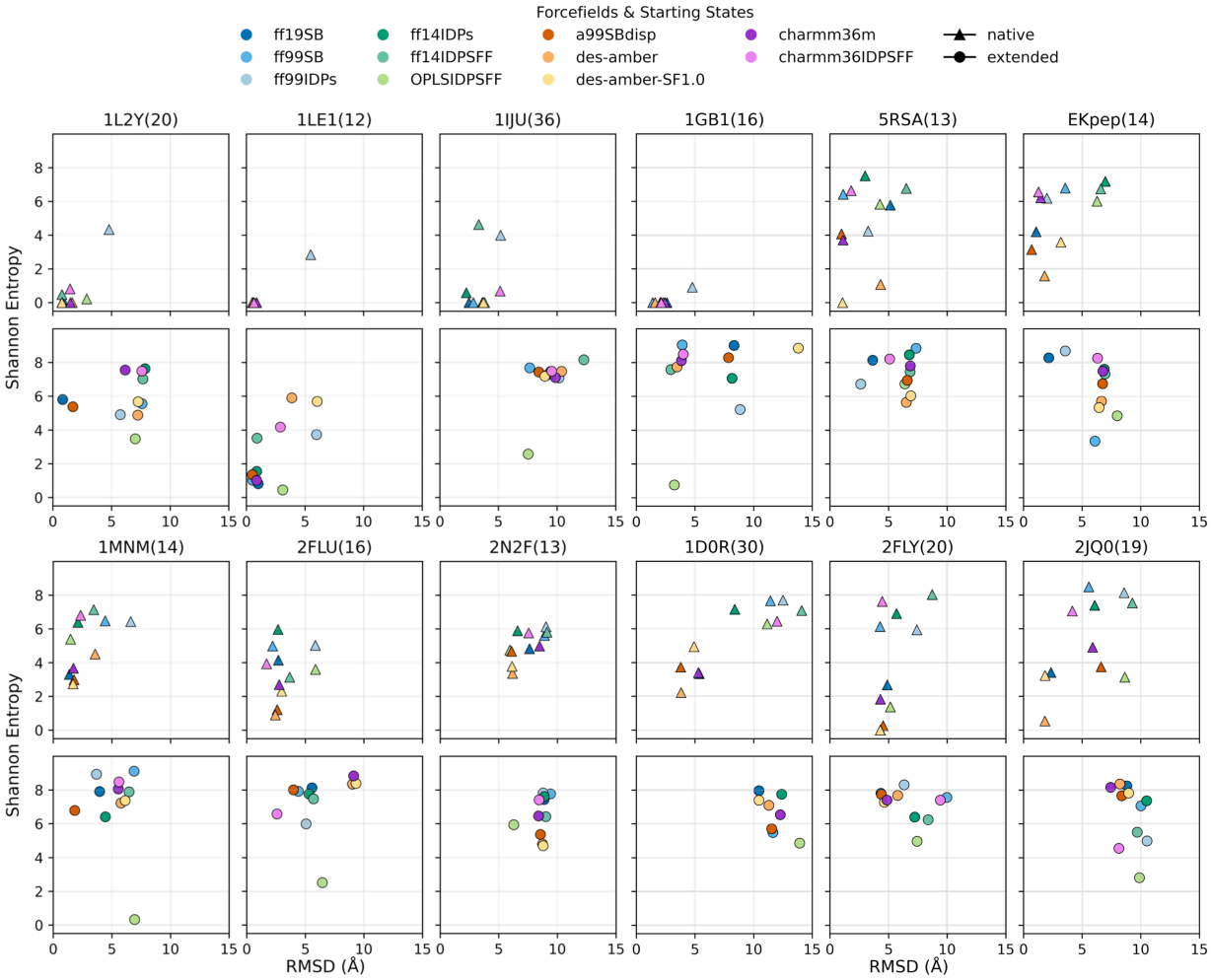

Figure 4: **Relationship between Shannon entropy and RMSD across different peptide systems for each force field.** For each system, triangle markers (top panels) represent data from 200 ns simulations initiated from experimentally folded structures, while circle markers (bottom panels) correspond to 10 μs simulations starting from linear peptide sequences. Numbers in parentheses indicate the length of each peptide sequence.

1) Stable native basin (low entropy, low RMSD); 2) Non-native traps (low entropy, high RMSD); 3)Broad exploration (high entropy, any RMSD). Entropy values are not normalized across systems and should be interpreted within each system's context.

Miniproteins (1L2Y, 1LE1, 1IJU):

In short simulations (200 ns) from native conformations, all three systems retain low RMSD ($4\mathring{A}$) and low entropy (1.0) under most force fields. FF99IDPs consistently shows higher RMSD and entropy, suggesting destabilization. In long simulations from extended chains, only ff19SB and a99SBdisp achieve partial folding of Trp-cage (1L2Y) from extended conformations. In contrast, the Trpzip (1LE1) fold is readily sampled by several force fields, resulting in low RMSD ($1.5\mathring{A}$) and low entropy (2.0) for several force fields. Interestingly, OPLSIDPSFF finds a non-native hairpin that is readily stabilized as seen by its lowest entropy, indicating that its β-bias might be unbalanced with respect to subtle sequence-dependent properties. None of the force fields successfully folds the larger β-defensin-1 (1IJU) within 10 μs, where even the top clusters have very low population (SI Fig. 13). Examination of secondary structure timeseries (SI Fig. 12) reveals long-lived hairpins, particularly in OPLSIDPSFF, but as most of the system remains disordered, this leads to overall low population clusters. Interestingly, most of the secondary structure sampled is incompatible with native-like secondary structure preferences.

Partially structured peptides (1GB1, 5RSA, EKpep):

1GB1 remains stable from the native state (low entropy and RMSD). OPLSIDPSFF shows especially low entropy, consistent with its known hairpin preference. Approximately half of the force fields recover folded-like clusters from extended states. In contrast, 5RSA and EKpep show higher entropies even when RMSD remains low, indicating dynamic exchange between folded and unfolded states. Only ff99IDPs and ff19SB recover native-like clusters for these two systems starting from extended. Interestingly, neither of these two force fields

was among those that fold 1GB1, suggesting there might be a slight bias towards helical states.

Structured upon binding (1MNM, 2FLU, 2N2F):

In native-start simulations, 1MNM and 2FLU retain native-like clusters but with moderate-to-high entropy, consistent with transient helicity in the absence of a binding partner. Few force fields succeed in refolding these systems from extended chains. For the chameleon 1MNM, OPLSIDPSFF and ff14IDPSFF favor the hairpin conformation, with OPLSIDPSFF sampling it at low entropy (contrasting with the high entropy in runs starting from the helical conformation). 2N2F remains disordered independently of the starting point, with high RMSD and moderate entropy, confirming that no dominant folded state is sampled. This contrasts with 1MNM and 2FLU supports a nuanced view of conformational selection versus induced fit. The latter two sample bound-like structures as top clusters (albeit with low populations and high entropy), implying that a complementary binding site could stabilize these conformations. In contrast, 2N2F appears to require interaction with its binding partner to access the native-like fold as the top state.

Solvent-sensitive helices (1D0R, 2FLY, 2JQO):

Native-start trajectories preserve helical structure to varying degrees (RMSD $< 5\mathring{A}$) with moderate entropy. Surprisingly, extended-start simulations show lower entropy despite longer duration, often converging to compact, non-native states (RMSD 6–10Å, entropy < 2) – with some force fields (ff19SB, charmm36m, des-amber, des-amber-SF1.0) stabilizing partial helices at one termini, with intrachain hydrophobic interactions collapsing the remainder of the sequence. These compact states are not unexpected: starting helices are stabilized in membrane-mimicking environments and expose hydrophobic side chains. In aqueous solvent, collapse likely reflects an entropic and enthalpic drive to shield hydrophobics from water, which in turn leads to low-entropy conformations that are structurally distinct from the

input helix.

Discussion

Peptides sit at the edge of stability: they lack the extensive tertiary contacts that stabilize globular proteins. Some peptides adopt stable structures under physiological conditions and are often classified as miniproteins. Others become structured only in specific contexts, such as in non-aqueous solvents, macromolecular crowding, or upon binding to a partner. This intermediate regime, between intrinsically disordered and stably folded, makes peptides a sensitive benchmark to detect and characterize force field biases. The peptides chosen for this study span this continuum, including well-folded systems, disordered peptides, and context-dependent examples.

As peptide therapeutics continue to gain traction in pharmaceutical research, it is critical to assess what improvements are needed in computational pipelines to reliably predict peptide binding. A useful decomposition of the binding free energy is:

$\Delta G_{bind} = (\Delta G^{protein}_{conformation} + \Delta G^{peptide}_{conformation}) + \Delta G_{interaction}$;

In practice, the protein's conformational penalty between the apo and holo state ($\Delta G^{protein}_{conformation}$) often cancels in relative binding comparisons ($\Delta\Delta G_{bind}$) between two peptides. However, the peptide's conformational free energy depends strongly on the force field's ability to model its unbound and bound ensembles accurately. When two peptides are differentially affected by force field errors—such as differing helix propensities or hairpin lengths—the resulting ΔG_{bind} can be significantly biased.

Our interest in this topic stems from efforts to predict peptide epitopes, their binding modes, and complex structures using data-guided simulations.[86–88] In this context, sparse experimental data guide the peptide to approach the protein binding site (typically within ∼8 Å, avoiding diffusion times that hinder binding simulations), allowing the force field and sampling to determine the binding pose and whether the peptide folds upon binding. We ob-

serve a consistent trend where weaker binders (micromolar and millimolar) require stronger guiding data to reproduce expected binding poses, whereas nanomolar binders typically recover experimental binding modes with significantly less data. In low-affinity binders, where the energetic contributions from folding and binding are comparable, even minor force field biases may disrupt the delicate balance required for productive complex formation – requiring higher guiding power.[89] Identifying such trends is important for going from qualitative relative binding affinities (e.g., from competitive binding simulations[86,90]) into more quantitative and robust measurements. The use of implicit solvent in previous methodologies inherits deficiencies from this force field selection. Thus, the current work helps users make better decisions for choosing force fields for transferring these methodologies into explicit solvent environments.

The force fields selected include both traditional parameterizations, originally optimized for folded proteins, and newer variants that aim to balance folded and disordered state sampling. Force field developers already benchmark their methods using metrics tailored to their development goals, often comparing simulated observables to experimental data such as NMR chemical shifts or scalar couplings,[91] with agreement quantified via χ^2 statistics. Additionally, studies that compare across an array of force fields are usually intended to identify alternative metrics or benchmarks that support more informed force field selection choices.[25,92? ? ,93] Such studies provide valuable insight into force field performance and underscore the complexity of assessing accuracy in molecular simulations.

One interesting note is that traditionally it has been easier to assess helicity than it is β propensity. Thus, many force field assessments have focused on whether the force field is too helical or not – looking at helical vs coil balance. However, it is entirely possible that a force field has either too much propensity to form both helices and strands,[20,94] or too little of both of them compared to coil conformations.

Our paired simulation design (starting from native or extended) allows us to distinguish between a force field's ability to preserve native conformations and its ability to discover

them from unfolded states. Several force fields (e.g., ff14IDPSFF, OPLSIDPSFF) maintain hairpins once formed but fail to reach them from extended structures—suggesting shallow but narrow basins. Others (e.g., ff19SB, ff99IDPs) allow reversible transitions, consistent with broader landscape exploration.

RMSD alone cannot distinguish between realistic flexibility and biased trapping. By analyzing Shannon entropy over cluster populations, we reveal whether force fields sample broad ensembles (suggesting realistic disorder) or artificially narrow basins (indicative of structural bias). For example, OPLSIDPSFF often shows low entropy across peptides, consistent with early stabilization of compact, non-native basins.

Our results indicate that no single force field performs best across all systems. Nonetheless, clear trends emerge. Some force fields exhibit a strong bias toward specific secondary structures, stabilizing helices or strands even when these are not experimentally favored. Others tend to sample transient structure without stabilizing it long enough to be biologically relevant. A third group largely suppresses structure formation, even in peptides expected to fold. These behaviors are informative of underlying biases and limitations.

In our simulations, OPLSIDPSFF consistently promotes β-hairpins even in systems like EK or GLP-1 that are not β-structured, highlighting a consistent strand bias. In contrast, ff99IDPs frequently destabilizes helices, even in stable miniproteins like Trp-cage, and occasionally introduces β-structure in disordered or helical systems. ff19SB and a99SBdisp, by contrast, maintain expected secondary structure in folded systems and allow context-sensitive folding in marginal peptides. Notably, force fields optimized for disordered ensembles do not consistently outperform traditional models. For example, ff14IDPSFF introduces non-native β-hairpins in several peptides, while OPLSIDPSFF frequently stabilizes strand-pairing even in helically biased systems. These results caution against assuming that IDP-tuned force fields generalize to all flexible peptide systems.

Based on stability, folding, and entropy behavior across twelve peptides, ff19SB and a99SBdisp consistently show the most balanced performance—preserving native folds, avoid-

ing over-stabilization, and sampling relevant ensembles. These force fields represent a strong starting point for modeling flexible peptides. Ongoing improvements in force field design, expanded benchmark sets, and longer simulations, combined with FAIR (Findable, Accessible, Interoperable, Reproducible) principles, offer new opportunities to detect and correct structural biases. Our benchmark shows that peptides, as sensitive probes between order and disorder, expose biases not always evident in globular protein models. We advocate for routine inclusion of diverse peptide benchmarks—covering miniproteins, disordered sequences, and context-dependent folders—in future evaluations.

Conclusion

Peptides inhabit a structurally diverse and biologically significant regime that challenges current molecular mechanics force fields. Our systematic benchmark, combining short simulations from native structures and long folding trajectories from extended chains, reveals that while many force fields are capable of maintaining folded states in select systems, few are unbiased across the full peptide landscape. Force fields such as ff19SB and a99SBdisp strike a useful balance—retaining native structure in well-folded systems while allowing transitions in marginal or context-sensitive peptides. Others, such as ff99IDPs or OPLSIDPSFF, show clear tendencies toward particular secondary structures, often stabilizing non-native folds.

These findings have important implications for peptide modeling in drug discovery, where ΔG predictions depend not only on interaction energies but also on accurate modeling of conformational ensembles. When comparing different peptides, force field-dependent errors in the conformational component of ΔG can bias binding predictions. Our results underscore the need for caution when interpreting peptide simulations and highlight the value of ensemble-based and comparative strategies.

We anticipate that this benchmark will serve both as a practical resource for force field users and as a testbed for future force field development targeting intrinsically disordered

and conformationally adaptive systems. The dataset, simulation protocols, and analysis framework are available at https://github.com/PDNALab/peptFF-benchmark to facilitate further refinement and standardization in the community.

Acknowledgement

The authors thank the support from the National Institutes of Health grant R01GM149646.

Supporting Information Available

Additional Figures can be found in the Supplementary information.

References

(1) Diella, F.; Haslam, N.; Chica, C.; Budd, A.; Michael, S.; Brown, N. P.; Trave, G.; Gibson, T. J.; others Understanding eukaryotic linear motifs and their role in cell signaling and regulation. *Front Biosci* **2008**, *13*, 603.

(2) Neduva, V.; Russell, R. B. Peptides mediating interaction networks: new leads at last. *Current opinion in biotechnology* **2006**, *17*, 465–471.

(3) Katuwawala, A.; Peng, Z.; Yang, J.; Kurgan, L. Computational prediction of MoRFs, short disorder-to-order transitioning protein binding regions. *Computational and Structural Biotechnology Journal* **2019**, *17*, 454–462.

(4) Lee, A. C.-L.; Harris, J. L.; Khanna, K. K.; Hong, J.-H. A comprehensive review on current advances in peptide drug development and design. *International journal of molecular sciences* **2019**, *20*, 2383.

(5) Chang, L.; Mondal, A.; Singh, B.; Martínez-Noa, Y.; Perez, A. Revolutionizing peptide-based drug discovery: Advances in the post-AlphaFold era. *Wiley Interdisciplinary Reviews: Computational Molecular Science* **2024**, *14*.

(6) Mollica, L.; Bessa, L. M.; Hanoulle, X.; Jensen, M. R.; Blackledge, M.; Schneider, R. Binding mechanisms of intrinsically disordered proteins: theory, simulation, and experiment. *Frontiers in molecular biosciences* **2016**, *3*, 52.

(7) Robustelli, P.; Piana, S.; Shaw, D. E. Mechanism of coupled folding-upon-binding of an intrinsically disordered protein. *Journal of the American Chemical Society* **2020**, *142*, 11092–11101.

(8) Luong, T. D.; Nagpal, S.; Sadqi, M.; Muñoz, V. A modular approach to map out the conformational landscapes of unbound intrinsically disordered proteins. *Proceedings of the National Academy of Sciences* **2022**, *119*, e2113572119.

(9) Milstein, M. L.; Kimler, V. A.; Ghatak, C.; Ladokhin, A. S.; Goldberg, A. F. An inducible amphipathic helix within the intrinsically disordered C terminus can participate in membrane curvature generation by peripherin-2/rds. *Journal of Biological Chemistry* **2017**, *292*, 7850–7865.

(10) Mondal, A.; Swapna, G.; Lopez, M. M.; Klang, L.; Hao, J.; Ma, L.; Roth, M. J.; Montelione, G. T.; Perez, A. Structure determination of challenging protein–peptide complexes combining NMR chemical shift data and molecular dynamics simulations. *Journal of chemical information and modeling* **2023**, *63*, 2058–2072.

(11) Kannan, S.; Lane, D. P.; Verma, C. S. Long range recognition and selection in IDPs: the interactions of the C-terminus of p53. *Scientific reports* **2016**, *6*, 23750.

(12) Patel, K.; Walport, L. J.; Walshe, J. L.; Solomon, P. D.; Low, J. K.; Tran, D. H.; Mouradian, K. S.; Silva, A. P.; Wilkinson-White, L.; Norman, A.; others Cyclic peptides

can engage a single binding pocket through highly divergent modes. *Proceedings of the National Academy of Sciences* **2020**, *117*, 26728–26738.

(13) Csizmok, V.; Follis, A. V.; Kriwacki, R. W.; Forman-Kay, J. D. Dynamic protein interaction networks and new structural paradigms in signaling. *Chemical reviews* **2016**, *116*, 6424–6462.

(14) Tesei, G.; Trolle, A. I.; Jonsson, N.; Betz, J.; Knudsen, F. E.; Pesce, F.; Johansson, K. E.; Lindorff-Larsen, K. Conformational ensembles of the human intrinsically disordered proteome. *Nature* **2024**, *626*, 897–904.

(15) Robustelli, P.; Piana, S.; Shaw, D. E. Developing a molecular dynamics force field for both folded and disordered protein states. *Proceedings of the National Academy of Sciences* **2018**, *115*, E4758–E4766.

(16) Jephthah, S.; Pesce, F.; Lindorff-Larsen, K.; Skepo, M. Force field effects in simulations of flexible peptides with varying polyproline II propensity. *Journal of chemical theory and computation* **2021**, *17*, 6634–6646.

(17) Palazzesi, F.; Prakash, M. K.; Bonomi, M.; Barducci, A. Accuracy of current all-atom force-fields in modeling protein disordered states. *Journal of chemical theory and computation* **2015**, *11*, 2–7.

(18) Matthes, D.; De Groot, B. L. Secondary structure propensities in peptide folding simulations: a systematic comparison of molecular mechanics interaction schemes. *Biophysical journal* **2009**, *97*, 599–608.

(19) Lincoff, J.; Sasmal, S.; Head-Gordon, T. The combined force field-sampling problem in simulations of disordered amyloid-β peptides. *The Journal of chemical physics* **2019**, *150*.

(20) Best, R. B.; Hummer, G. Optimized Molecular Dynamics Force Fields Applied to the HelixCoil Transition of Polypeptides. *The journal of physical chemistry. B* **2009**, *113*, 9004 – 9015.

(21) Perez, A.; MacCallum, J. L.; Brini, E.; Simmerling, C.; Dill, K. A. Grid-based backbone correction to the ff12SB protein force field for implicit-solvent simulations. *Journal of chemical theory and computation* **2015**, *11*, 4770–4779.

(22) Rahman, M. U.; Rehman, A. U.; Liu, H.; Chen, H.-F. Comparison and evaluation of force fields for intrinsically disordered proteins. *Journal of chemical information and modeling* **2020**, *60*, 4912–4923.

(23) Yu, L.; Li, D.-W.; Bruschweiler, R. Systematic differences between current molecular dynamics force fields to represent local properties of intrinsically disordered proteins. *The Journal of Physical Chemistry B* **2021**, *125*, 798–804.

(24) Lopes, P. E.; Guvench, O.; MacKerell Jr, A. D. *Molecular modeling of proteins*; Springer, 2014; pp 47–71.

(25) Beauchamp, K. A.; Lin, Y.-S.; Das, R.; Pande, V. S. Are protein force fields getting better? A systematic benchmark on 524 diverse NMR measurements. *Journal of chemical theory and computation* **2012**, *8*, 1409–1414.

(26) Neidigh, J. W.; Fesinmeyer, R. M.; Andersen, N. H. Designing a 20-residue protein. *Nature structural biology* **2002**, *9*, 425 – 430.

(27) Cochran, A. G.; Skelton, N. J.; Starovasnik, M. A. Tryptophan zippers: stable, monomeric beta -hairpins. *Proceedings of the National Academy of Sciences of the United States of America* **2001**, *98*, 5578 – 5583, trpzip2 ACE SER TRP THR TRP GLU ASN GLY LYS TRP THR TRP LYS NME.

(28) Hoover, D. M.; Chertov, O.; Lubkowski, J. The structure of human β-defensin-1: new insights into structural properties of β-defensins. *Journal of Biological Chemistry* **2001**, *276*, 39021–39026.

(29) Gronenborn, A. M.; Filpula, D. R.; Essig, N. Z.; Achari, A.; Whitlow, M.; Wingfield, P. T.; Clore, G. M. A novel, highly stable fold of the immunoglobulin binding domain of streptococcal protein G. *Science* **1991**, *253*, 657–661.

(30) Wlodawer, A.; Borkakoti, N.; Moss, D.; Howlin, B. Comparison of two independently refined models of ribonuclease-A. *Structural Science* **1986**, *42*, 379–387.

(31) Sommese, R. F.; Sivaramakrishnan, S.; Baldwin, R. L.; Spudich, J. A. Helicity of short E-R/K peptides. *Protein Science* **2010**, *19*, 2001–2005.

(32) Tan, S.; Richmond, T. J. Crystal structure of the yeast MATα2/MCM1/DNA ternary complex. *Nature* **1998**, *391*, 660–666.

(33) Lo, S.; Li, X.; Henzl, M. T.; Beamer, L. J.; Hannink, M. Structure of the Keap1:Nrf2 interface provides mechanistic insight into Nrf2 signaling. *The EMBO Journal* **2006**, *25*, 3605–3617.

(34) O'Connor, C.; White, K. L.; Doncescu, N.; Didenko, T.; Roth, B. L.; Czaplicki, G.; Stevens, R. C.; Wüthrich, K.; Milon, A. NMR structure and dynamics of the agonist dynorphin peptide bound to the human kappa opioid receptor. *Proceedings of the National Academy of Sciences* **2015**, *112*, 11852–11857.

(35) Chang, X.; Keller, D.; Bjørn, S.; Led, J. J. Structure and folding of glucagon-like peptide-1-(7–36)-amide in aqueous trifluoroethanol studied by NMR spectroscopy. *Magnetic Resonance in Chemistry* **2001**, *39*, 477–483.

(36) Lucyk, S.; Taha, H.; Yamamoto, H.; Miskolzie, M.; Kotovych, G. NMR conformational

analysis of proadrenomedullin N-terminal 20 peptide, a proangiogenic factor involved in tumor growth. *Biopolymers: Original Research on Biomolecules* **2006**, *81*, 295–308.

(37) Resende, J. M.; Moraes, C. M.; Prates, M. V.; Cesar, A.; Almeida, F. C.; Mundim, N. C.; Valente, A. P.; Bemquerer, M. P.; Piló-Veloso, D.; Bechinger, B. Solution NMR structures of the antimicrobial peptides phylloseptin-1,-2, and-3 and biological activity: the role of charges and hydrogen bonding interactions in stabilizing helix conformations. *Peptides* **2008**, *29*, 1633–1644.

(38) Tian, C.; Kasavajhala, K.; Belfon, K. A.; Raguette, L.; Huang, H.; Migues, A. N.; Bickel, J.; Wang, Y.; Pincay, J.; Wu, Q.; others ff19SB: amino-acid-specific protein backbone parameters trained against quantum mechanics energy surfaces in solution. *Journal of chemical theory and computation* **2019**, *16*, 528–552.

(39) Hornak, V.; Abel, R.; Okur, A.; Strockbine, B.; Roitberg, A.; Simmerling, C. Comparison of multiple Amber force fields and development of improved protein backbone parameters. *Proteins: Structure, Function, and Bioinformatics* **2006**, *65*, 712–725.

(40) Huang, J.; Rauscher, S.; Nawrocki, G.; Ran, T.; Feig, M.; De Groot, B. L.; Grubmüller, H.; MacKerell Jr, A. D. CHARMM36m: an improved force field for folded and intrinsically disordered proteins. *Nature methods* **2017**, *14*, 71–73.

(41) Wang, W.; Ye, W.; Jiang, C.; Luo, R.; Chen, H.-F. New force field on modeling intrinsically disordered proteins. *Chemical biology & drug design* **2014**, *84*, 253–269.

(42) Song, D.; Wang, W.; Ye, W.; Ji, D.; Luo, R.; Chen, H.-F. ff14IDPs force field improving the conformation sampling of intrinsically disordered proteins. 2017.

(43) Song, D.; Luo, R.; Chen, H.-F. The IDP-specific force field ff14IDPSFF improves the conformer sampling of intrinsically disordered proteins. *Journal of chemical information and modeling* **2017**, *57*, 1166–1178.

(44) Liu, H.; Song, D.; Zhang, Y.; Yang, S.; Luo, R.; Chen, H.-F. Extensive tests and evaluation of the CHARMM36IDPSFF force field for intrinsically disordered proteins and folded proteins. *Physical Chemistry Chemical Physics* **2019**, *21*, 21918–21931.

(45) Yang, S.; Liu, H.; Zhang, Y.; Lu, H.; Chen, H. Residue-specific force field improving the sample of intrinsically disordered proteins and folded proteins. *Journal of Chemical Information and Modeling* **2019**, *59*, 4793–4805.

(46) Piana, S.; Robustelli, P.; Tan, D.; Chen, S.; Shaw, D. E. Development of a force field for the simulation of single-chain proteins and protein–protein complexes. *Journal of chemical theory and computation* **2020**, *16*, 2494–2507.

(47) Izadi, S.; Anandakrishnan, R.; Onufriev, A. V. Building water models: a different approach. *The journal of physical chemistry letters* **2014**, *5*, 3863–3871.

(48) Jorgensen, W. L.; Chandrasekhar, J.; Madura, J. D.; Impey, R. W.; Klein, M. L. Comparison of simple potential functions for simulating liquid water. *The Journal of chemical physics* **1983**, *79*, 926–935.

(49) Piana, S.; Donchev, A. G.; Robustelli, P.; Shaw, D. E. Water dispersion interactions strongly influence simulated structural properties of disordered protein states. *The journal of physical chemistry B* **2015**, *119*, 5113–5123.

(50) Lindahl, E.; Abraham, M. J.; Hess, B.; van der Spoel, D. GROMACS 2019.2 Manual. 2019.

(51) Case, D.; Belfon, K.; Ben-Shalom, I.; Brozell, S.; Cerutti, D.; Cheatham III, T.; Cruzeiro, V.; Darden, T.; Duke, R.; Giambasu, G.; others AMBER 20. 2020. *San Francisco: University of California.[Google Scholar]*

(52) Case, D. A.; Aktulga, H. M.; Belfon, K.; Ben-Shalom, I. Y.; Berryman, J. T.;

Brozell, S. R.; Cerutti, D. S.; Cheatham III, T. E.; Cisneros, G. A.; Cruzeiro, V. W. D.; others *Amber 2023*; University of California, San Francisco, 2023.

(53) Maier, J. A.; Martinez, C.; Kasavajhala, K.; Wickstrom, L.; Hauser, K. E.; Simmerling, C. ff14SB: improving the accuracy of protein side chain and backbone parameters from ff99SB. *Journal of chemical theory and computation* **2015**, *11*, 3696–3713.

(54) Jo, S.; Kim, T.; Iyer, V. G.; Im, W. CHARMM-GUI: a web-based graphical user interface for CHARMM. *Journal of computational chemistry* **2008**, *29*, 1859–1865.

(55) Brooks, B. R.; Brooks III, C. L.; Mackerell Jr, A. D.; Nilsson, L.; Petrella, R. J.; Roux, B.; Won, Y.; Archontis, G.; Bartels, C.; Boresch, S.; others CHARMM: the biomolecular simulation program. *Journal of computational chemistry* **2009**, *30*, 1545–1614.

(56) Lee, J.; Cheng, X.; Jo, S.; MacKerell, A. D.; Klauda, J. B.; Im, W. CHARMM-GUI input generator for NAMD, GROMACS, AMBER, OpenMM, and CHARMM/OpenMM simulations using the CHARMM36 additive force field. *Biophysical journal* **2016**, *110*, 641a.

(57) Pastor, R. W.; Brooks, B. R.; Szabo, A. An analysis of the accuracy of Langevin and molecular dynamics algorithms. *Molecular Physics* **1988**, *65*, 1409–1419.

(58) Wu, X.; Brooks, B. R. Self-guided Langevin dynamics simulation method. *Chemical physics letters* **2003**, *381*, 512–518.

(59) Wu, X.; Brooks, B. R.; Vanden-Eijnden, E. Self-guided L angevin dynamics via generalized L angevin equation. *Journal of computational chemistry* **2016**, *37*, 595–601.

(60) Berendsen, H. J.; Postma, J. v.; Van Gunsteren, W. F.; DiNola, A.; Haak, J. R. Molecular dynamics with coupling to an external bath. *The Journal of chemical physics* **1984**, *81*, 3684–3690.

(61) Berman, H. M.; Westbrook, J.; Feng, Z.; Gilliland, G.; Bhat, T. N.; Weissig, H.; Shindyalov, I. N.; Bourne, P. E. The protein data bank. *Nucleic acids research* **2000**, *28*, 235–242.

(62) Press, W. H.; Teukolsky, S. A.; Vetterling, W. T.; Flannery, B. P. Numerical recipes 3rd edition. *Cambridge: New York* **2007**,

(63) Hess, B. P-LINCS: A parallel linear constraint solver for molecular simulation. *Journal of chemical theory and computation* **2008**, *4*, 116–122.

(64) Essmann, U.; Perera, L.; Berkowitz, M. L.; Darden, T.; Lee, H.; Pedersen, L. G. A smooth particle mesh Ewald method. *The Journal of chemical physics* **1995**, *103*, 8577–8593.

(65) Parrinello, M.; Rahman, A. Crystal structure and pair potentials: A molecular-dynamics study. *Physical review letters* **1980**, *45*, 1196.

(66) Parrinello, M.; Rahman, A. Strain fluctuations and elastic constants. *The Journal of Chemical Physics* **1982**, *76*, 2662–2666.

(67) Hopkins, C. W.; Le Grand, S.; Walker, R. C.; Roitberg, A. E. Long-time-step molecular dynamics through hydrogen mass repartitioning. *Journal of chemical theory and computation* **2015**, *11*, 1864–1874.

(68) Roe, D. R.; Cheatham III, T. E. PTRAJ and CPPTRAJ: software for processing and analysis of molecular dynamics trajectory data. *Journal of chemical theory and computation* **2013**, *9*, 3084–3095.

(69) Roe, D. R.; Cheatham III, T. E. Parallelization of CPPTRAJ enables large scale analysis of molecular dynamics trajectory data. 2018.

(70) Gowers, R. J.; Linke, M.; Barnoud, J.; Reddy, T. J. E.; Melo, M. N.; Seyler, S. L.;

Domanski, J.; Dotson, D. L.; Buchoux, S.; Kenney, I. M.; others *MDAnalysis: a Python package for the rapid analysis of molecular dynamics simulations*; 2019.

(71) Michaud-Agrawal, N.; Denning, E. J.; Woolf, T. B.; Beckstein, O. MDAnalysis: a toolkit for the analysis of molecular dynamics simulations. *Journal of computational chemistry* **2011**, *32*, 2319–2327.

(72) Humphrey, W.; Dalke, A.; Schulten, K. VMD: visual molecular dynamics. *Journal of molecular graphics* **1996**, *14*, 33–38.

(73) Ramachandran, G. N. Stereochemistry of polypeptide chain configurations. *J. Mol. Biol.* **1963**, *7*, 95–99.

(74) Kabsch, W.; Sander, C. Dictionary of protein secondary structure: pattern recognition of hydrogen-bonded and geometrical features. *Biopolymers: Original Research on Biomolecules* **1983**, *22*, 2577–2637.

(75) Shannon, C. E. A mathematical theory of communication. *The Bell system technical journal* **1948**, *27*, 379–423.

(76) McKinney, W.; others Data structures for statistical computing in Python. *scipy* **2010**, *445*, 51–56.

(77) Harris, C. R.; Millman, K. J.; Van Der Walt, S. J.; Gommers, R.; Virtanen, P.; Cournapeau, D.; Wieser, E.; Taylor, J.; Berg, S.; Smith, N. J.; others Array programming with NumPy. *nature* **2020**, *585*, 357–362.

(78) Sawai, M. V.; Jia, H. P.; Liu, L.; Aseyev, V.; Wiencek, J. M.; McCray, P. B.; Ganz, T.; Kearney, W. R.; Tack, B. F. The NMR Structure of Human -Defensin-2 Reveals a Novel -Helical Segment † , ‡. *Biochemistry* **2001**, *40*, 3810–3816.

(79) Chang, L.; Perez, A. Deciphering the Folding Mechanism of Proteins G and L and Their Mutants. *Journal of the American Chemical Society* **2022**, *144*, 14668–14677.

(80) Shoemaker, K. R.; Kim, P. S.; Brems, D. N.; Marqusee, S.; York, E. J.; Chaiken, I. M.; Stewart, J. M.; Baldwin, R. L. Nature of the charged-group effect on the stability of the C-peptide helix. *Proceedings of the National Academy of Sciences of the United States of America* **1985**, *82*, 2349 – 2353, c-peptide LYS GLU THR ALA ALA ALA LYS PHE GLU ARG GLN HIS HSE ribo ALA GLU THR ALA ALA ALA LYS PHE LEU ARG ALA HIE ALA c-peptide LYS GLU THR ALA ALA ALA LYS PHE GLU ARG GLN HIS HSE ribo ALA GLU THR ALA ALA ALA LYS PHE LEU ARG ALA HIE ALA.

(81) Brüschweiler, R.; Morikis, D.; Wright, P. E. Hydration of the partially folded peptide RN-24 studied by multidimensional NMR. *Journal of biomolecular NMR* **1995**, *5*, 353 356, ribonuclease ribonuclease.

(82) Sommese, R. F.; Sivaramakrishnan, S.; Baldwin, R. L.; Spudich, J. A. Helicity of short E-R/K peptides. *Protein Science* **2010**, *19*, 2001 – 2005.

(83) Jumper, J.; Evans, R.; Pritzel, A.; Green, T.; Figurnov, M.; Ronneberger, O.; Tunyasuvunakool, K.; Bates, R.; Žídek, A.; Potapenko, A.; others Highly accurate protein structure prediction with AlphaFold. *nature* **2021**, *596*, 583–589.

(84) Candotti, M.; Pérez, A.; Ferrer-Costa, C.; Rueda, M.; Meyer, T.; Gelpí, J. L.; Orozco, M. Exploring Early Stages of the Chemical Unfolding of Proteins at the Proteome Scale. *PLoS Computational Biology* **2013**, *9*, e1003393.

(85) Perez, A.; Orozco, M. Real-time atomistic description of DNA unfolding. *Angewandte Chemie (International ed. in English)* **2010**, *49*, 4805 – 4808.

(86) Morrone, J. A.; Perez, A.; MacCallum, J.; Dill, K. A. Computed binding of peptides to proteins with MELD-accelerated molecular dynamics. *Journal of chemical theory and computation* **2017**, *13*, 870–876.

(87) Lang, L.; Perez, A. Binding Ensembles of p53-MDM2 Peptide Inhibitors by Combining Bayesian Inference and Atomistic Simulations. *Molecules* **2021**, *26*, 198.

(88) Mondal, A.; Swapna, G.; Lopez, M. M.; Klang, L.; Hao, J.; Ma, L.; Roth, M. J.; Montelione, G. T.; Perez, A. Structure determination of challenging protein–peptide complexes combining NMR chemical shift data and molecular dynamics simulations. *Journal of chemical information and modeling* **2023**, *63*, 2058–2072.

(89) Singh, B.; Mondal, A.; Gaalswyk, K.; MacCallum, J. L.; Perez, A. MELD-Adapt: On-the-Fly Belief Updating in Integrative Molecular Dynamics. *Journal of Chemical Theory and Computation* **2024**, *20*, 9230–9242.

(90) Parui, S.; Robertson, J. C.; Somani, S.; Tresadern, G.; Liu, C.; Dill, K. A. MELD-Bracket Ranks Binding Affinities of Diverse Sets of Ligands. *Journal of Chemical Information and Modeling* **2023**, *63*, 2857–2865.

(91) Koes, D. R.; Vries, J. K. Evaluating amber force fields using computed NMR chemical shifts. *Proteins: Structure, Function, and Bioinformatics* **2017**, *85*, 1944–1956.

(92) Sarthak, K.; Winogradoff, D.; Ge, Y.; Myong, S.; Aksimentiev, A. Benchmarking Molecular Dynamics Force Fields for All-Atom Simulations of Biological Condensates. *Journal of Chemical Theory and Computation* **2023**, *19*, 3721–3740.

(93) Huggins, D. J. Comparing the Performance of Different AMBER Protein Forcefields, Partial Charge Assignments, and Water Models for Absolute Binding Free Energy Calculations. *Journal of Chemical Theory and Computation* **2022**, *18*, 2616–2630.

(94) Best, R. B.; Mittal, J. Balance between and Structures in Ab Initio Protein Folding. *The journal of physical chemistry. B* **2010**, *114*, 8790 – 8798.

TOC Graphic

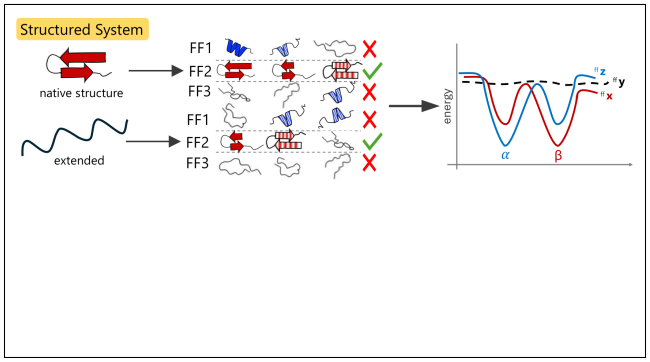
Structured System
native structure
extended
FF1
FF2
FF3
FF1
FF2
FF3
energy
z
y
x
α
β